Journal of Physical Science
Vol. 37(1), 43–62, 2026

Effect of Sintering Temperature on the Physical and Chemical Properties of Titanium-Hydroxyapatite Composite Incorporated with Commercial and Synthesised 45S5 Bioactive Glass

Dayana Syafiqah Abu Bakar,[1] Muralithran Govindan Kutty[1] and Noor Azlin Yahya[1*]

[1]*Department of Restorative Dentistry, Faculty of Dentistry, Universiti Malaya, 50603 Kuala Lumpur, Malaysia*

*Corresponding author: nazlin@um.edu.my

Published online: 29 April 2026

To cite this article: Abu Bakar, D. S., Kutty, M. G. & Yahya, N. A. (2026). Effect of sintering temperature on the physical and chemical properties of titanium-hydroxyapatite composite incorporated with commercial and synthesised 45S5 bioactive glass. *J. Phys. Sci.*, 37(1), 43–62. https://doi.org/10.21315/jps2026.37.1.3

To link this article: https://doi.org/10.21315/jps2026.37.1.3

ABSTRACT: The titanium-hydroxyapatite (Ti-HA) composite is promising for dental use due to Ti's strength and corrosion resistance, and HA's biocompatibility. However, high-temperature sintering can oxidise Ti and decompose HA. This study explores using bioactive glass (BG) as a sintering aid to preserve these properties while lowering sintering temperatures. The research objective is to compare the variations caused by sintering temperature Ti-HA incorporating 45S5 BG (synthesised and commercially available) in terms of chemical and physical properties. The synthesis of 45S5 BG was done via melt-quench method while the Ti-HA and Ti-HA-BG composites via powder metallurgy with a ratio of 50:50 and 45:45:10 in weight percentages (wt.%), respectively. Four temperature variations (900°C, 1,000°C, 1,100°C and 1,200°C) were applied during atmospheric furnace sintering. Chemical analysis utilised X-ray diffractometry (XRD) and Fourier Transform Infrared Reflectance (FTIR), while physical analysis examined density and volumetric change. XRD confirmed HA was detected in the samples of Ti-HA system with the incorporation of 45S5 BG, particularly from 900°C–1,000°C for commercial BG and only at 900°C for synthesised BG composites. However, HA was not detected in the Ti-HA system without BG. Physical analysis indicated that densities and volumetric expansion of the composites were not significantly influenced by the sample batch or sintering temperature. Overall, the fabrication of 45S5 BG powder and its incorporation into the Ti-HA composite demonstrated the potential of 45S5 BG as a viable sintering aid. Based on XRD results, Ti-HA composite samples incorporated with commercial BG and sintered at 900°C exhibited optimal outcomes.

Keywords: titanium, hydroxyapatite, 45S5 bioactive glass, powder metallurgy, sintering

1. INTRODUCTION

Biomaterials play a crucial role in healthcare, particularly in dentistry and medicine. In dentistry, these materials are categorised into four primary classes: (1) polymers, (2) ceramics, (3) metals and (4) composites. Biocomposites for oral and dental tissue engineering have been created in particular by utilising the compatible properties of various material mixtures.[1,2] Composite materials, by definition, combine two or more materials with differing properties to create unique composite properties.[3,4] Restoring endodontically treated teeth, especially those with significant structural loss, has long been a challenge in dentistry. Dental posts are employed when the remaining tooth structure cannot offer sufficient support for restorations.[5] While metals like stainless steel, titanium (Ti), chromium and cobalt have historically been used for dental posts due to their commendable mechanical attributes, each material presents drawbacks such as corrosion susceptibility in stainless steel and retrieval challenges with Ti.[6,7]

In response to limitations with metallic alternatives, non-metallic options like fiber-reinforced composite posts have emerged. These posts exhibit properties such as modulus of elasticity similar to dentin, high retention and good force transmission. However, concerns remain regarding their limited stiffness and vulnerability to heavy loads.[6,7] Titanium-hydroxyapatite (Ti-HA) composites have garnered significant attention for dental posts due to Ti's excellent mechanical properties and corrosion resistance, combined with HA's similarity to tooth and bone composition. However, fabricating Ti-HA composites poses challenges due to high-temperature sintering processes, leading to material alterations.[8–10]

During the high-temperature sintering process of Ti-HA composites, several undesirable reactions may occur, including the production of tetra-calcium phosphate (TTCP: $Ca_4(PO_4)_2O$), tri-calcium phosphate (TCP: $Ca_3(PO_4)_2$), titanium oxide (TiO_2) and calcium titanate ($CaTiO_3$). Arifin et al. observed the emergence of two distinct calcium phosphate phases (TTCP and TCP) during the sintering of Ti-HA composites, subsequent to the dehydroxylation and decomposition of pure HA.[8] Dehydroxylation initiated at approximately 900°C in an air environment, slightly earlier at about 850°C in a moisture-free atmosphere. The dehydrated water within the HA composite triggered a reaction with Ti ions, leading to the production of TiO_2. This interaction accelerated the dehydroxylation and decomposition of HA, commencing at around 800°C. Simultaneously, oxidation of Ti occurred during the sintering process, with temperatures ranging from 700°C–1,200°C. TiO_2 was produced at approximately 800°C, resulting in the formation of only two crystalline phases, TiO_2 and $CaTiO_3$.[8]

One promising solution to these challenges is incorporating low-melting-point additives like bioactive glass (BG) as sintering aid. BG reduces sintering temperatures without compromising mechanical or biological properties.[10,11] Abdulmunem et al. investigated various sintering temperatures and percentages of BG (containing; silicon dioxide [SiO_2], sodium oxide [NaO], calcium oxide [CaO], boron trioxide [B_2O_3], phosphorus pentoxide [P_2O_5], calcium floride [CaF_2], magnesium oxide [MgO] and TiO_2) incorporation into Ti-HA composites.[12] Their findings showed that incorporating 10% BG into the Ti-HA system allowed for reduced sintering temperatures while preserving essential properties. The use of an atmospheric furnace for sintering produced superior results compared to vacuumed furnaces, including increased compression strength, enhanced microhardness and improved modulus of elasticity.

In this study, a specific type of BG, 45S5, was selected due to its well-established bioactivity and chemical composition of 46.1 mol.% SiO_2, 24.4 mol.% Na_2O, 26.9 mol.% CaO and 2.6 mol.% P_2O_5. Commercially recognised as Bioglass®, 45S5 was first developed by Hench in 1969 and has since been widely used in biomedical applications. To evaluate its impact on the Ti-HA-BG composite, both synthesised and commercially available 45S5 BG powders were used, following the optimum ratio and atmospheric furnace method suggested by Abdulmunem et al.[12] This approach allows for a direct comparison of how variations in BG morphology and particle size affect the composite's properties, particularly in response to different sintering temperatures.

By incorporating 45S5 BG into the Ti-HA system, this study evaluates its effect on densification, phase stability and bioactivity. The findings provide insights into the consolidation mechanism and highlight its role in optimising the sintering process. Additionally, this approach could reduce manufacturing costs by enabling lower sintering temperatures and simplifying production, making Ti-HA-BG composites more efficient and scalable for biomedical applications.

In this context, Ti provides strength, HA replicates natural tooth composition and BG enhances bonding with surrounding tissues. The strategic combination of these materials and optimised sintering are key to developing durable and biocompatible dental posts. This study suggests that such an approach can enhance dental treatment durability and effectiveness, marking a significant advancement in biomaterials.

2. EXPERIMENTAL

2.1 Samples Preparation

The 45S5 BG powder was synthesised following the melt-quenching process described by Zarifah et al.[11] Four different materials of raw powder oxides with specific weight percentages of 45% SiO_2, 24.5% CaO, 24.5% Na_2O and 6% P_2O_5 were milled together using a planetary ball milling machine (XQM-(2.6)L, Changsha, China) with zirconia balls and ceramic jars at 100 rpm for 4 h. The milling process throughout this study was conducted with a ball-to-sample mass ratio of 1:10 to ensure effective mixing and particle size reduction. The resulting powder was then subjected to a melting process in an atmosphere furnace (XINYOO-17000, Henan, China) at 1,380°C for 3 h with a heating rate of 10°C/min. After melting, the sample was rapidly quenched in water, and the resulting frits were dried overnight at room temperature. Subsequently, the glass frits were crushed into a powdered form using a mortar and pestle, followed by further processing in a planetary ball mill machine to ensure homogeneity and achieve the desired particle size distribution.

Commercially available Ti powder (R&M Chemicals) with an average particle size of 45 μm, HA powder (Sigma-Aldrich) with an average particle size of 5 μm, and 45S5 BG powder (XL Sci-Tech, Inc.) with particle sizes ranging from 45 μm–75 μm were used to prepare the composite samples. The study involved three batches of composite samples: Batch A (control group, Ti-HA), Batch B (experimental group with commercially obtained BG, Ti-HA-BG) and Batch C (experimental group with synthesised BG, Ti-HA-BG). Each batch comprised 20 samples, divided equally into four groups based on sintering temperatures: 900°C, 1,000°C, 1,100°C and 1,200°C, with five samples per group. This temperature range was selected to ensure the minimisation of Ti oxidation and HA decomposition. As mentioned in Table 1, powders were weighed according to the weight percentage for each sample batch respectively and milled using a planetary ball milling machine for 5 h at 100 rpm. Sample compaction was achieved using a hydraulic hand press machine (OL57 Manfredi, Italy) and stainless steel molds, applying a force of 1,500 psi to form cylindrical pellets with a diameter of approximately 3 cm and a height of 2.5 cm. Sintering was performed in an atmosphere furnace (XINYOO-1700, Henan, China) with a 4 h hold time and a gradual heating rate of 5°C/min. After sintering, the samples were allowed to cool overnight in the furnace before extraction.

Table 1: Samples composition in weight percentage (wt%)

Sample batch	Titanium (wt%)	Hydroxyapatite (wt%)	Commercial 45S5 bioactive glass (wt%)	Synthesised 45S5 bioactive glass (wt%)
Batch A	50	50	–	–
Batch B	45	45	10 wt%	–
Batch C	45	45	–	10

2.2 Sample Characterisation

2.2.1 Chemical analysis

Crystalline phase identification was performed using X-ray Diffraction (XRD) with a PANalytical EMPYREAN instrument (Lelyweg Almelo, Netherlands). X'Pert HighScore software (X'Pert Pro, Panalytical, Almelo, Netherlands) was utilised to analyse the XRD pattern and data, with reference to the Joint Committee of Powder Diffraction Standard-International Center for Diffraction Data (JCPDS-ICCD) files for phase identification. Fourier Transform Infrared Spectroscopy-Attenuated Total Reflectance (FTIR-ATR) analysis was conducted using a Thermoscientific Nicolet 6700 instrument (Massachusetts, USA) in the wave number range of 1,850 cm^{-1}–650 cm^{-1} at room temperature and 0.5 cm^{-1} resolution. The FTIR-ATR analysis aimed to identify the functional groups present in the prepared composites. The specific spectral range was selected to focus on the key vibrational bands associated with silicate and phosphate groups, which are most relevant to the structural analysis in this study. XRD and FTIR analysis were employed to characterise both commercial and synthesised BG powder, as well as the composite samples.

2.2.2 Physical analysis

The particle size distribution (PSD) analysis of both commercial and synthesised 45S5 BG powder was conducted using a particle size analyser machine (Zetasizer Nano S, Worcestershire, UK), with 10 replicate samples analysed for both types of BG powder. The analysis process involved sieving BG powders prior to dispersing them in a liquid medium, specifically water, as it is commonly used to simulate body fluids, allowing for accurate measurement while minimising the impact of BG dissolution over the short analysis period. The Zetasizer Nano S utilised light sources to illuminate the samples and the scattered light was then detected to determine the particle size. The obtained data was processed and analysed using the dedicated software provided by Zetasizer (Malvern Instrument, Worcestershire, UK). This software generated a distribution plot that depicted the percentage of particles within specific size ranges.

Meanwhile, density measurements of samples composites were obtained by using Archimedes' principle, with distilled water as the buoyant medium. A densitometer (Sartorius AX224, Goettingen, Germany) was used for weight measurements. Density was calculated using the formula:

$$\rho = [w_a/(w_a - w_b)] \times \rho_b \quad (1)$$

where,

ρ = sample density
w_a = weight of sample in air (g)
w_b = weight of sample in buoyant (g)
ρ_b = density of the buoyant (gcm^{-3})

Volumetric changes were determined using a digital vernier caliper (Mitutoyo/ Digimatic, Tokyo, Japan) to measure the dimensions and calculate the difference in volume between the green and sintered materials using the formula:

$$VC = [(Vs - Vg) / Vg] \times 100\% \quad (2)$$

where,

VC = volumetric change (%)
Vs = volume of sintered samples (cm^3)
Vg = volume of green samples (cm^3)

In this study, 60 samples were divided into three batches, each containing 20 samples. Each batch was further equally distributed across four sintering temperature groups: (1) 900°C, (2) 1,000°C, (3) 1,100°C and (4) 1,200°C, with five samples per group. The results for density and volumetric change were averaged within each batch. The results of density and volumetric change of samples composites were also subjected to descriptive and analytical statistical analysis using SPSS software (version 12.0.1, SPSS Inc, Chicago, IL, USA). Two-way analysis of variance (ANOVA) was employed to evaluate the effects of sample batch, sintering temperature, and their interactions on density and volumetric change.

3. RESULTS AND DISCUSSION

Figures 1–4 present the samples from each batch across the four different sintering temperatures: 900°C, 1,000°C, 1,100°C and 1,200°C. All samples remained intact and free of cracks across all sintering temperature groups after the sintering process.

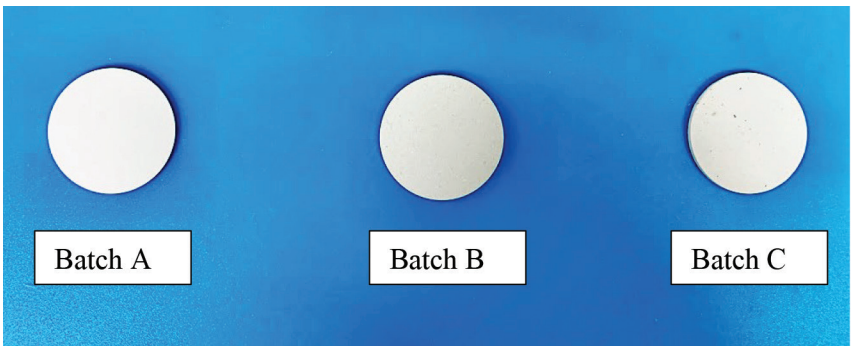

Figure 1: Sintered sample of each batch at 900°C.

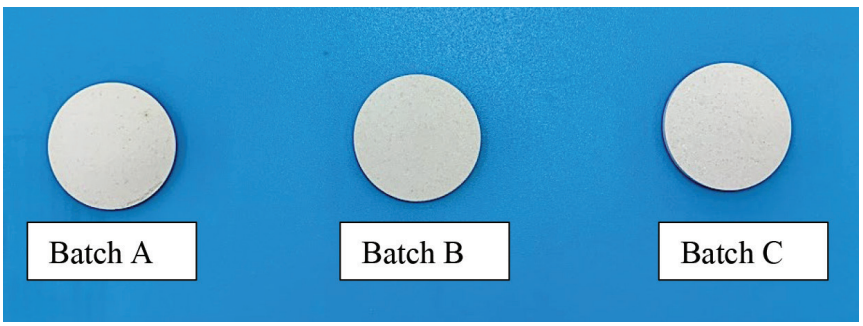

Figure 2: Sintered sample of each batch at 1,000°C.

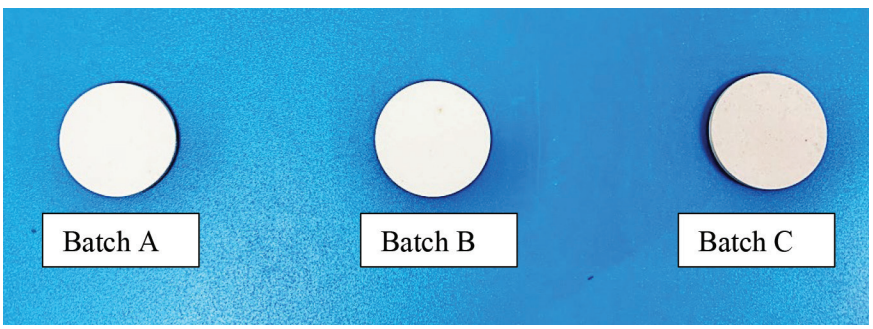

Figure 3: Sintered sample of each batch at 1,100°C.

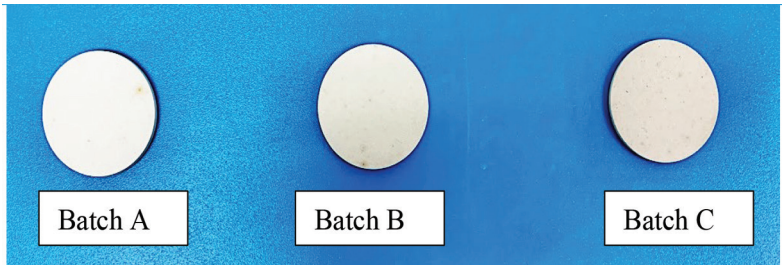

Figure 4: Sintered sample of each batch at 1,200°C.

3.1 Chemical Analysis

The XRD spectra of both BG powders (see Figure 5) exhibited a similar trend, suggesting a typical amorphous structure of silicate glass. The broad peaks indicated the glassy phase. In comparison, commercial BG particle XRD patterns were dispersive, with no sharp diffraction peaks, whereas synthesised BG powders had some sharp peaks. These results indicated that during synthesis of 45S5 BG, the quenching process occurred rapid enough below the glass transition temperature (T_g) to create the amorphous solid structure.[13] The glass T_g is a crucial characteristic of BG as explained by Khurshid et al.[14] T_g represents the temperature at which an amorphous solid transitions into a supercooled liquid state during the heating process. In order to manufacture glass, a material is rapidly cooled from a supercooled liquid, which is a transitional state between a liquid and a glass. The material is cooled to below a critical temperature, referred to as the T_g, in order to become an amorphous solid. T_g is employed as a characterisation parameter for BG because it indirectly reflects the glass network structure, which is associated with essential properties of the glass. These properties include solubility, degradation, mechanical properties and crystallisation.

XRD patterns of synthesised BG also showed the presence of amorphous glassy phase and crystalline phases of combeite ($Na_2Ca_2Si_3O_9$) and wollastonite ($CaSiO_3$) as the major and minor crystalline phase, respectively. The justification of the ease of crystallisation of the BG can be associated with the existence of phosphate and silicate network, as well as the possibility of crystalline phase separation even on a micro scale of the two crystalline phases depending on heat treatment parameters. The addition of even a slight percentage of P_2O_5 to silicate glasses can also promote the volume nucleation. Volume nucleation refers to the process of initiating the formation of new crystalline phases within a glass material throughout its entire volume. It involves the nucleation of crystals in various regions of the glass matrix, leading to the growth of multiple crystalline phases. Thus, due to the presence of these silicate and phosphate in the glass system, crystallisation in the BG is quite likely to occur.[15–17]

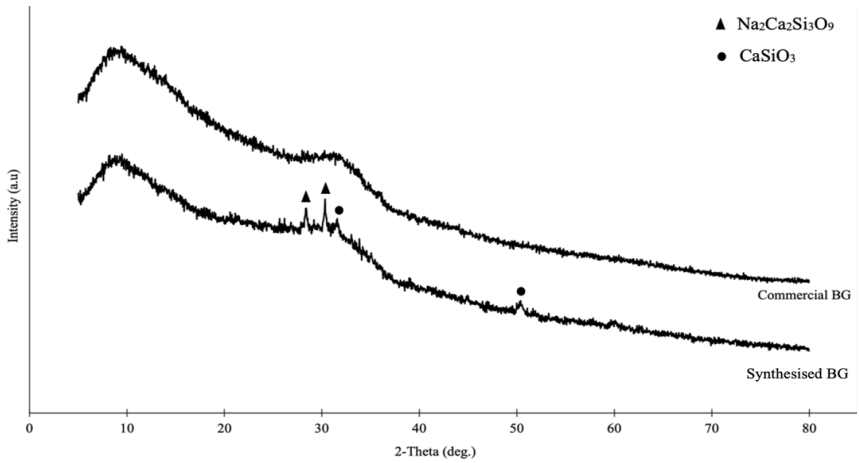

Figure 5: XRD of commercial and synthesised BG powders.

Figure 6 shows the FTIR spectra of commercial BG and the synthesised BG powder. The absorption spectra of commercial BG showed a broad band at 892.14 cm^{-1} and another broad band at 1,436.54 cm^{-1}. On the other hand, the absorption spectra of synthesised BG showed one broad band at 895.35 cm^{-1}. The characteristic peaks of commercial BG and synthesised BG at ~890 cm^{-1} correspond to the vibration of Si-O-Si stretching of non-bridging oxygen atoms.[13,18] Based on these FTIR results, both commercial and synthesised BG confirmed their amorphous nature, as generally observed in amorphous silica glasses, the Si-O-Si stretching, Si-O-Si bending and Si-O stretching modes, was detected.[13] Moreover, the crystallisation of the major phase combeite was verified by the higher intensity of the Si-O-Si band in the synthesised BG, as in agreement with the previously discussed XRD results.

Both commercial and synthesised BG powders revealed FTIR absorption spectra which are known and accepted to be mainly characteristic of silicate network. This is mainly due to the existence of significant SiO_2 as a basic building constituent, which comprises of 45% of the system. The FTIR absorption spectra of the BGs did not reveal separate bands because of the combined existence of phosphate network, which could be attributed to the low percentage of P_2O_5, which comprises only 6% of the BG constituent. Some phosphate band modes have been shown to vibrate at 500 cm^{-1}–600 cm^{-1} for P-O bending and 800 cm^{-1}–120 cm^{-1} for P-O stretching.[15,19]

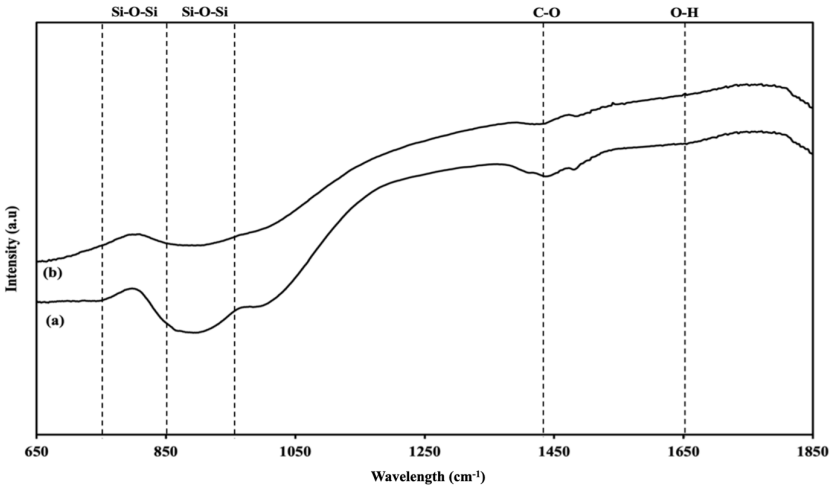

Figure 6: FTIR spectra (a) commercial BG and (b) synthesised BG.

These regions are already occupied by the main silicate network vibrations, thus the weaker phosphate network vibrations are expected to be super-imposed. The weak band at ~1,460 cm^{-1} can be attributed to the C-O vibrational mode, which indicates the presence of purely ionic carbonate-like structures with high symmetry which are likely adsorbed on the glass surface upon reaction with CO_2 in air, while the weak band at ~1,650 cm^{-1} can be attributed to molecular water adsorbed on surface.[15,20–22]

Figures 7–9 depict the XRD patterns of sample composite Batch A, B and C, respectively. In Batch A, the XRD pattern indicated the presence of TCP (JCPDS card no. 00-009-0348) and TTCP (JCPDS card no. 00-025-1137) as the predominant phases, alongside partial decomposition of HA (JCPDS card no. 00-009-0432) and oxidation of Ti (JCPDS card no. 00-044-1294). This decomposition of HA and Ti oxidation are commonly observed at elevated temperatures ranging from 700°C to 1,200°C.[8–10,23] The absence of materials aiding in the sintering process, such as BG, may contribute to these undesirable reactions.[9,24] In contrast, XRD patterns of Batch B and Batch C, which included 45S5 BG, revealed predominant phases of HA and TTCP, with minor phases of HA and Ti. Although HA decomposition and Ti oxidation were still observed, the interactions between Ti and HA were effectively minimised, leading to the absence of $CaTiO_3$ formation.[25] The presence of HA was detected only in samples with BG incorporation (Batch B and Batch C), with Batch B showing HA presence from 900°C–1,000°C and Batch C at 900°C only. Ti was detected as a

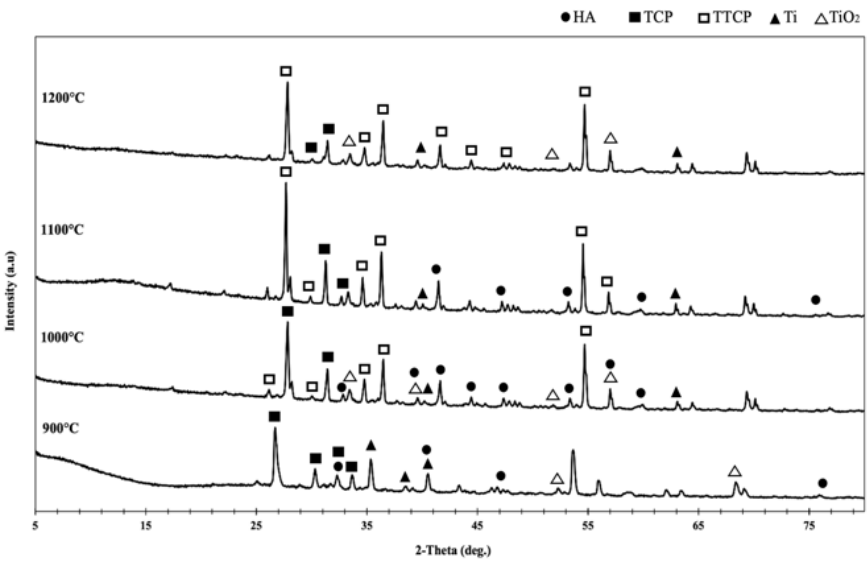

Figure 7: XRD of Batch A with different sintering temperatures.

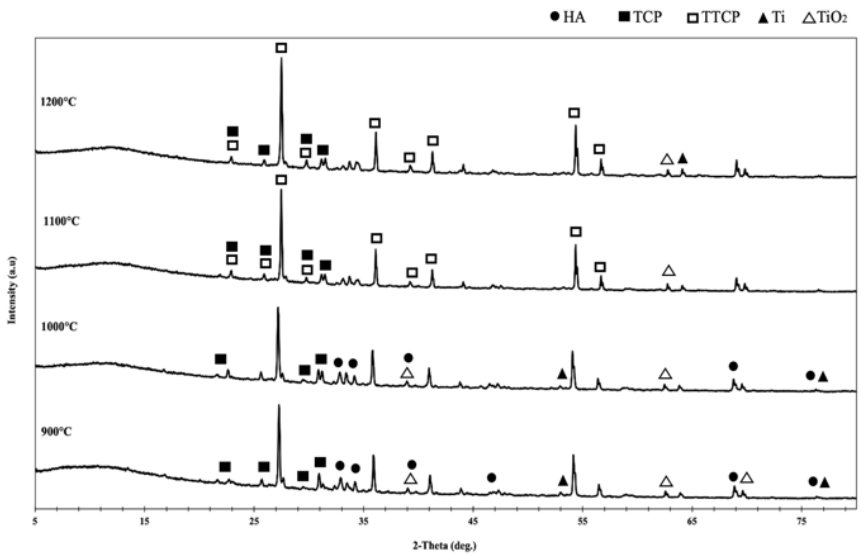

Figure 8: XRD of Batch B with different sintering temperatures.

minor phase in all samples across each batch. Overall, the incorporation of 45S5 BG into Ti-HA composites and sintering at 900°C resulted in a stable composite below the decomposition temperature of HA and Ti oxidation. Minor HA decomposition and Ti oxidation were observed in both Batch B and Batch C, contrasting with Batch A, where major HA decomposition occurred at the same sintering temperature. These findings are consistent with previous studies demonstrating HA decomposition into TCP and Ti oxidation into Ti_xP_y and $CaTiO_3$ at elevated temperatures.[9,10] Various studies on Ti-HA-BG systems have shown enhancements in bioactivity and properties with BG incorporation. Abdulmunem et al. has discovered a decrease in sintering temperature to 900°C with 10% BG incorporation without compromising Ti and HA properties.[12]

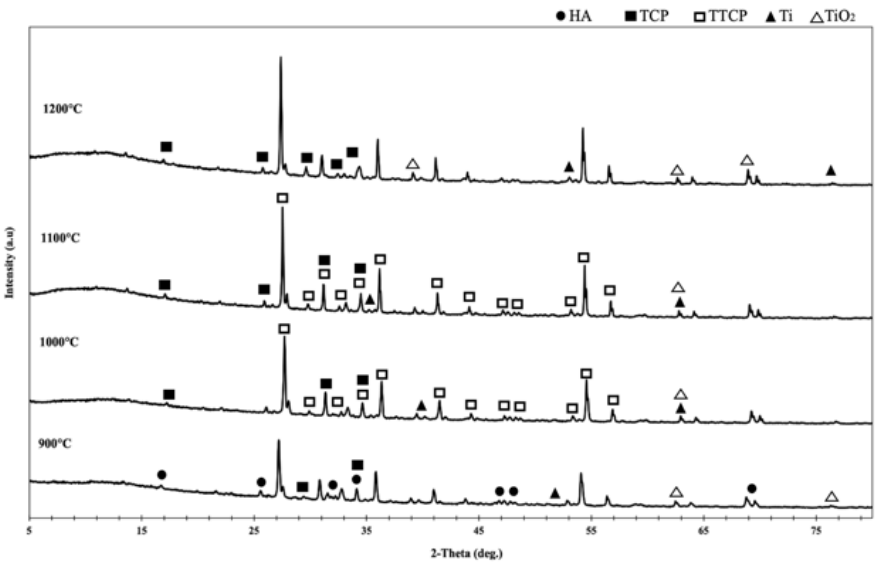

Figure 9: XRD of Batch C with different sintering temperatures.

Figures 10–12 depict the FTIR patterns of sample Batch A, B and C, respectively. The absorption spectra of Batch A at 900°C, 1,000°C, 1,100°C and 1,200°C show a broad band at 1,012.35 cm^{-1}, 971.88 cm^{-1}, 1,003.56 cm^{-1} and 1,015.15 cm^{-1}, respectively. Batch B shows broad band of absorption spectra at G1 and G2 that were observed at 1,027.10 cm^{-1} and 979.92 cm^{-1}, respectively. The characteristic peaks at 1,000 cm^{-1}–1,100 cm^{-1} correspond to the vibration of Si-O-Si symmetric stretching of bridging oxygen atoms within tetrahedra while the characteristic peaks at 860 cm^{-1}–940 cm^{-1} correspond to the vibration of Si-O-Si stretching of non-bridging oxygen atoms.[13,18] In this study, FTIR reflectance spectra shows the characteristic peaks that correspond to the vibration of Si-O-Si symmetric stretching of bridging oxygen atoms within

tetrahedra which is very strong at 1,000 cm^{-1}–1,100 cm^{-1} region, causing in the overlapping with the stretching PO_4 vibrational peak. Theoretically, phosphate ions (PO_4^{3-}) have four vibration modes; v_1, v_2, v_3 and v_4, all of which are infrared active.[26] For sintered composites in Batch A, the FTIR spectrum indicated the elimination of phosphate peaks due to the removal of HA during the sintering process. The elimination of PO_4^{3-} bands demonstrated the complete decomposition of Ca_xP_y phases to an amorphous phase and CaO which may have further resulted in formation of $CaTiO_3$ and $CaCO_3$.[26] On the other hand, FTIR spectrum of Batch B shows the bands in the region of 900 cm^{-1}–1,100 cm^{-1} almost vanished with increasing temperature.[10,26]

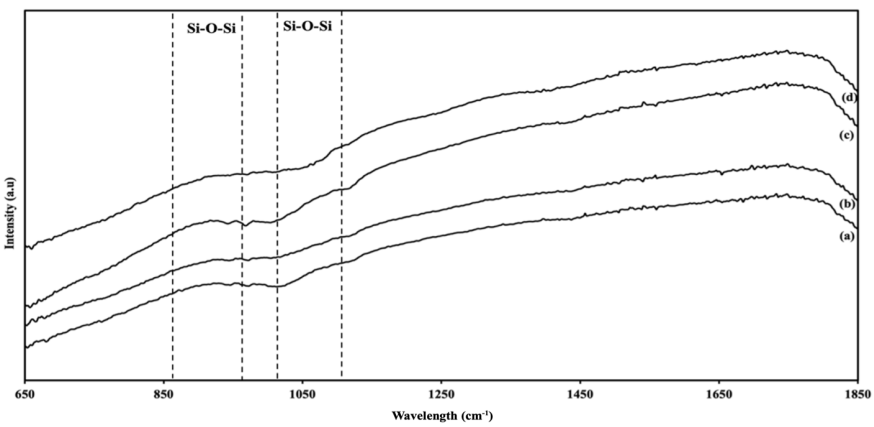

Figure 10: FTIR Spectra of Batch A with different sintering temperatures: (a) 900°C, (b) 1,000°C, (c) 1,100°C and (d) 1,200°C.

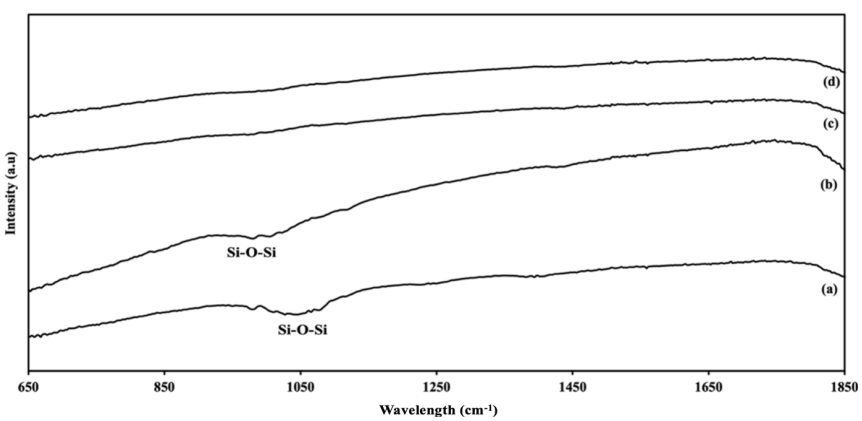

Figure 11: FTIR Spectra of Batch B with different sintering temperatures: (a) 900°C (b) 1,000°C, (c) 1,100°C and (d) 1,200°C.

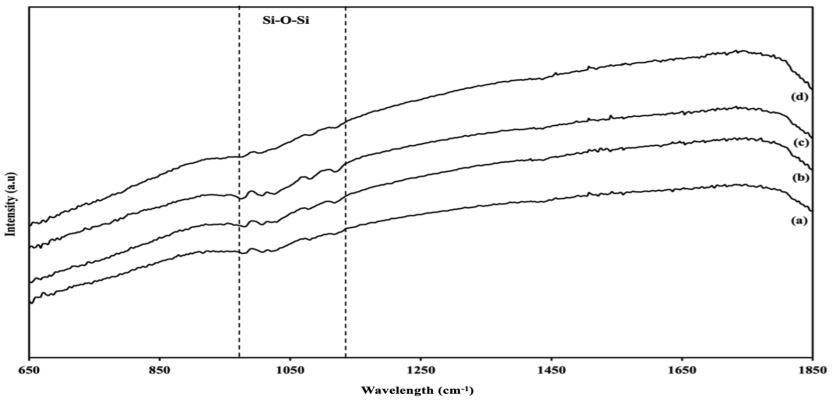

Figure 12: FTIR Spectra of Batch C with different sintering temperatures: (a) 900°C (b) 1,000°C, (c) 1,100°C and (d) 1,200°C.

3.2 Physical Analysis

Figure 13(a) and 13(b) show the PSD analysis of the commercial BG and synthesised BG respectively. The PSD analysis for commercial BG showed bimodal distribution while the PSD of fabricated BG showed unimodal distribution. The bimodal distribution of Figure 13(a) consisted of two peaks. The major peak with 83.8% of the total samples consisted of the average particle size of 197.4 nm, whereas the minor peak showed 16.2% of the total sample with particles size of 65.42 nm. The average PSD of commercial BG was calculated resulting in a measurement of 176.02 nm. On the other hand, Figure 13(b) showed that the synthesised BG particles were bigger than the commercial BG with the particle size of 1,396 nm. Particle size is closely related to the surface area of the glass particles. Larger particles possess a smaller surface area where as the smaller particles have more surface area per unit volume that is exposed to the surrounding area. The surface area of BG powders increases as the particle size decreases. This increased surface area can lead to enhanced interactions between the BG powder and biological properties. This can also lead to improved bioactivity.[27] In this study, it was observed that after milling the glass frits of fabricated BG, the resulting particles presented higher average of particle size than the commercial BG powders. The difference in the size of particles might be due to the commercial BG powders were produced using different starting materials and different manufacturing technique. Environmental factors and different brands providing the powder may also affect the properties of the material particles.

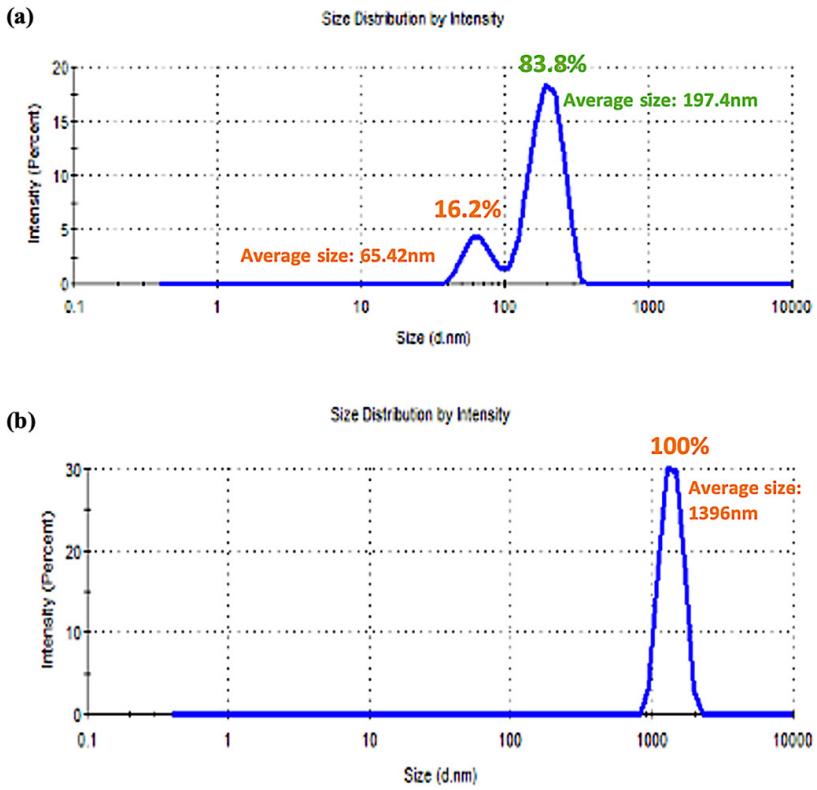

Figure 13: PSD of (a) commercial BG and (b) synthesised BG powders.

The highest density value recorded for Batch A is sintered at 1,100°C with 3.21 gcm^{-3}, while the lowest density value the density recorded is sintered 1,200°C with 3.11 gcm^{-3}. For Batch B, the highest density value recorded is sintered at 1,100°C with 3.10 gcm^{-3} while lowest density value recorded is sintered 1,200°C with 3.01 gcm^{-3}. In Batch C, the highest density value recorded is sintered at 1,000°C with 3.07 gcm^{-3} while the lowest density value recorded is sintered 1,200°C with 2.97 gcm^{-3}. The experimental densities of Batch A, B and C fluctuated with the increasing sintering temperature. This is likely to happen due to the grain growth. As the sintering temperature increases, the grains within the material tend to grow. This grain growth can result in densification of the material, leading to an increase in density. However, if excessive grain growth occurs, it can lead to coarsening of the microstructure and a decrease in density. At elevated sintering temperatures, the rate of densification increases, leading to moderate to high grain growth in the composites. Differences in initial grain sizes create forces at the grain boundaries, promoting grain growth. When grain boundaries experience tension due to this movement, pores have the potential to relocate through

volume or surface diffusion, or even through evaporation-condensation across the pores. However, to retain the alignment of the pores along with the grain boundaries, precise control of the heating rate is necessary.[28]

A two-way ANOVA was conducted to further assess the impact of sample batch and sintering temperature on density and volumetric change. Sample batch, comprising Batch A, Batch B, and Batch C, and sintering temperature levels (900°C, 1,000°C, 1,100°C and 1,200°C) were considered as independent variables. The results, as presented in Table 2, indicated no significant interaction between sample batch and sintering temperature on density ($F[6, 48] = 0.237$, $p = 0.962 > 0.05$). However, sample batch exhibited a statistically significant effect on density ($p = 0.000 < 0.05$), whereas sintering temperature did not significantly impact density ($p = 0.075 > 0.05$), as revealed by simple main effects analysis. The density of the specimens is influenced by various factors, such as the properties of the powders and the conditions during compaction. In this study, the compaction conditions were kept consistent for all specimens, meaning that the green density was primarily determined by the characteristics of the powders. The Ti particles exhibited varying sizes and there was a notable difference in particle size between the Ti and HA powders. As a result, the mixture of Ti and HA powders could effectively achieve a multi-modal packing. This means that the smaller HA particles could readily fill the spaces between the larger Ti particles, resulting in a more compact structure.[28]

Table 2: Two-way ANOVA for the effect of sample batch and sintering temperature on density

Source	Type III sum of squares	df	Mean square	F	Sig.
Corrected model	0.308a	11	0.028	2.663	0.009
Intercept	566.229	1	566.229	53788.275	0.000
Sample batch	0.216	2	0.108	10.269	0.000
Sintering temperature	0.077	3	0.026	2.444	0.075
Sample batch * Sintering temperature	0.015	6	0.002	0.237	0.962
Error	0.505	48	0.011		
Total	567.043	60			
Corrected total	0.814	59			

Note: df = degree of freedom; Sig. = significance value (p-value); R2 = 0.379 (adjusted R2 = 0.237).

This study also observed an expansion in the volumetric change of the composite across all batches. Batch A recorded the highest volumetric expansion (VE) sintered at 1,200°C with 14.65% while the lowest VE was recorded for samples sintered at 1,000°C with 7.42%. Batch B recorded the highest VE sintered at 900°C with 21.27% and the lowest VE was recorded sintered at 1,200°C with 13.17%. Batch C recorded the highest VE sintered at 900°C with 27.23% while the lowest VE was recorded sintered at 1,200°C with 10.07%. Overall, Batch C at 900°C showed highest expansion with 27.23% while Batch A at 1,000°C showed lowest expansion with 7.42%. Based on the ANOVA results in Table 3, no statistically significant interaction between sample batch and sintering temperature on VE ($F[6, 1.315] = 0.237$, $p = 0.269 > 0.05$). However, sample batch demonstrated a statistically significant effect on VE ($p = 0.017 < 0.05$) according to simple main effects analysis. Conversely, sintering temperature did not exhibit a statistically significant effect on VE ($p = 0.056 > 0.05$) based on simple main effects analysis. The expansion occurred might be due to the agglomeration of HA particles during the sintering process which creates empty spaces known as pores. These pores, formed due to the irregular shape of the powder particles, cannot be entirely eliminated during the grain enlargement process, resulting in the formation of closed pores.[28] The air trapped within these closed pores expands, leading to elongation of the sintered component.

Table 3: Two-way ANOVA for the effect of sample batch and sintering temperature on VE

Source	Type III sum of squares	df	Mean square	F	Sig.
Corrected model	1651.482a	11	150.135	2.263	0.026
Intercept	14831.436	1	14831.436	223.555	0.000
Sample batch	589.512	2	294.756	4.443	0.017
Sintering temperature	538.621	3	179.540	2.706	0.056
Sample batch * Sintering temperature	523.348	6	87.225	1.315	0.269
Error	3184.488	48	66.344		
Total	19667.406	60			
Corrected total	4835.970	59			

Note: $R^2 = 0.341$ (Adjusted $R^2 = 0.191$)

Another contributing factor to expansion is the significant mismatch between crystal lattice parameters of initial and subsequent phases, resulting in defects like vacancies, dislocations and stacking faults at particle interfaces. This mismatch can negatively impact the material, by reducing structural integrity, which may lead to fractures or poor bonding with surrounding tissues, affecting its long-term performance in

dental applications.[12,29] This structural instability can further drive expansion. Critical parameters in powder metallurgy sintering, such as maximum sintering temperature, sintering time at peak temperature and heating/cooling rates, significantly influence densification. Inadequate fusion and low densification can result from low sintering temperatures and insufficient duration, while improper cooling rates, influenced by factors like fan speed and atmosphere flow, may contribute to rapid expansion.[29]

4. CONCLUSION

The study successfully synthesised 45S5 BG powder using the melt-quench method and compared it with commercial 45S5 BG. Both types of BG were confirmed to have an amorphous phase through XRD. The synthesised BG powder exhibited a higher average of PSD compared to the commercial BG. Furthermore, this study investigated the comparison of Ti-HA and Ti-HA-BG composites that were sintered at four different sintering temperatures in terms of chemical and physical properties. Chemical analysis revealed that samples incorporating BG and sintered at lower temperatures showed better results compared to the Ti-HA. XRD analysis indicated the presence of HA only in the Ti-HA systems with the incorporation of BG, while the Ti-HA system without BG did not detect the presence of HA. The physical analysis revealed that the density and VE of the composites were not significantly influenced by the interaction between the sample batch and sintering temperature. In summary, the study successfully fabricated BG powder, characterised its properties and demonstrated the benefits of incorporating BG into Ti-HA composites. Notably, based on XRD results, Ti-HA composite samples incorporated with commercial BG and sintered at 900°C exhibited optimal outcomes.

5. ACKNOWLEDGEMENTS

This research was supported by the Fundamental Research Grant Scheme No. DP KPT FRGS/1/2017/SKK14/UM/02/4

6. REFERENCES

1. Ciocca, B. E. *et al.* (2019). Viability assays of PLLA fibrous membranes produced by rotary jet spinning for application in tissue engineering. *Braz. Arch. Biol. Technol.*, 62. https://doi.org/10.1590/1678-4324-2019170775
2. Mohanty, A. K., Misra, M. & Hinrichsen, G. (2000). Biofibres, biodegradable polymers and biocomposites: an overview. *Macromol. Mater. Eng.,* 276–277(1), 1–24. https://doi.org/10.1002/(SICI)1439-2054(20000301)276:1%3C1::AID-MAME1%3E3.0.CO;2-W

3. Furtos, G. et al. (2015). Biocomposites for orthopedic and dental application. *Key. Eng. Mater.*, 672, 261–275. https://doi.org/10.4028/www.scientific.net/KEM.672.261
4. Yıldızhan, Ş. et al. (2018). Bio-composite materials: A short review of recent trends, mechanical and chemical properties, and applications. *Eur. Mech. Sci.*, 2(3), 83–91. https://doi.org/10.26701/ems.369005
5. Abu Kasim, N. H. et al. (2011). 3D-FE analysis of functionally graded structured dental posts. *Dent. Mater. J.*, 30(6), 869–880. https://doi.org/10.4012/dmj.2010-161
6. Schwartz, R. S. & Robbins, J. W. (2004). Post placement and restoration of endodontically treated teeth: a literature review. *J. Endod.*, 30(5), 289–301. https://doi.org/10.1097/00004770-200405000-00001
7. Terry, D. A. & Swift, E. J. (2010). Post-and-cores: Past to present. *Int. Dent. SA*, 12(2), 1–28.
8. Arifin, A. et al. (2014). Material processing of hydroxyapatite and titanium alloy (HA/Ti) composite as implant materials using powder metallurgy: A review. *Mater. Des.*, 55, 165–175. https://doi.org/10.1016/j.matdes.2013.09.045
9. Balbinotti, P. et al. (2011). Microstructure development on sintered Ti/HA biocomposites produced by powder metallurgy. *Mater. Res.*, 14(3), 384–393. https://doi.org/10.1590/S1516-14392011005000044
10. Ning, C. & Zhou, Y. (2004). On the microstructure of biocomposites sintered from Ti, HA and bioactive glass. *Biomater.*, 25(17), 3379–3387. https://doi.org/10.1016/j.biomaterials.2003.10.017
11. Zarifah, N. A. et al. (2016). Effect of hydroxyapatite reinforced with 45S5 glass on physical, structural and mechanical properties. *Procedia Chem.*, 19, 30–37. https://doi.org/10.1016/j.proche.2016.03.008
12. Abdulmunem, M. et al. (2021). The effect of bioactive glass and sintering conditions on the properties of titanium-hydroxyapatite composites. *Sains Malays.*, 50(4), 1089–1099. https://doi.org/10.17576/jsm-2021-5004-19
13. Ismail, N., Mohamad, H. & Ahmad, N. (2020). Fabrication and characterization of 45S5 bioactive glass microspheres. *AIP Conf. Proc.*, 2267, 020041. https://doi.org/10.1063/5.0015700
14. Khurshid, Z. et al. (2019). Novel techniques of scaffold fabrication for bioactive glasses. *Key. Eng. Mater.*, 10(4), 599–609. https://doi.org/10.1002/jbm.b.33443
15. ElBatal, F. H. & ElKheshen, A. (2008). Preparation and characterization of some substituted bioglasses and their ceramic derivatives from the system SiO2-Na2O-CaO-P2O5 and effect of gamma irradiation. *Mater. Chem. Phys.*, 110(2–3), 352–362. https://doi.org/10.1016/j.matchemphys.2008.02.011
16. Majhi, M. R., Pyare, R. & Singh, S. P. (2012). Studies on preparation and characterizations of CaO-Na2O-SiO2-P2O5 bioglass ceramics substituted with Al_2O_3, TiO2 and ZrO2. *J. Biomater. Tissue Eng.*, 2(2), 154–169. https://doi.org/10.1166/jbt.2012.1032
17. Zarifah, N. A. et al. (2015). An elucidating study on physical and structural properties of 45S5 glass at different sintering temperatures. *J. Non. Cryst. Solids.*, 412, 24–29. https://doi.org/10.1016/j.jnoncrysol.2015.01.005

18. ElBatal, H. A. et al. (2003). Characterization of some bioglass-ceramics. *Mater. Chem. Phys.*, 80(3), 599–609. https://doi.org/10.1016/S0254-0584(03)00082-8
19. Jastrzbski, W. et al. (2011). Infrared spectroscopy of different phosphates structures. *Spectrochim. Acta. A. Mol. Biomol. Spectrosc.*, 79(4), 722–727. https://doi.org/10.1016/j.saa.2010.08.044
20. Cerruti, M. et al. (2005). Surface modifications of bioglass immersed in TRIS-buffered solution. A multitechnical spectroscopic study. *J. Phys. Chem.,* 109(30), 14496–14505. https://doi.org/10.1021/jp050705t
21. Cerruti, M. & Morterra, C. (2004). Carbonate formation on bioactive glasses. *Langmuir*., 20(15), 6382–6388. https://doi.org/10.1021/la049723c
22. Du, R. L. et al. (2007). Hydroxyapatite and bioactive glass composite coating on Ti_6Al_4V. *Key. Eng. Mater*., 330–332, 589–592. https://doi.org/10.4028/www.scientific.net/KEM.330-332.589
23. Shahrjerdi, A., et al. (2011). Fabrication of functionally graded hydroxyapatite-titanium by applying optimal sintering procedure and powder metallurgy. *Int. J. Phys. Sci*., 6(9), 2258–2267.
24. Weinand, W. R., Gonçalves, F. F. R. & Lima, W. M. (2006). Effect of sintering temperature in physical-mechanical behaviour and in titanium-hydroxyapatite composite sinterability. *Mater. Sci. Forum*., 530–531, 249–254. https://doi.org/10.4028/www.scientific.net/MSF.530-531.249
25. Beherei, H. H., Mohamed, K. R. & El-Bassyouni, G. T. (2009). Fabrication and characterization of bioactive glass (45S5)/titania biocomposites. *Ceram Int*., 35(5), 1991–1997. https://doi.org/10.1016/j.ceramint.2008.10.014
26. Ye, H., Liu, X. Y. & Hong, H. (2009). Characterization of sintered titanium/hydroxyapatite biocomposite using FTIR spectroscopy. *J. Mater. Sci. Mater. Med*., 20(4), 843–850. https://doi.org/10.1007/s10856-008-3647-3
27. Mabroum, H. et al. (2022). The effect of bioactive glass particle size and liquid phase on the physical-chemical and mechanical properties of carbonated apatite cement. *Ceram. Int*., 48(19), 28207–28220. https://doi.org/10.1016/j.ceramint.2022.06.126
28. Thangamani, N., Chinnakali, K. & Gnanam, F. D. (2002). The effect of powder processing on densification, microstructure and mechanical properties of hydroxyapatite. *Ceram. Int*., 28(4), 355–362. https://doi.org/10.1016/S0272-8842(01)00102-X
29. Wakily, H., Dabbagh, A., Abdullah, H., Abdul Halim, N. F. & Abu Kasim, N. H. (2015). Improved thermal and mechanical properties in hydroxyapatite-titanium composites by incorporating silica-coated titanium. *Mater. Lett*., 143, 322–325. https://doi.org/10.1016/j.matlet.2014.12.092